

Local structure of $\text{YNi}_2\text{B}_2\text{C}$ superconductor determined by x-ray-absorption spectroscopy

A. Yu. Ignatov and N. Ali

Department of Physics, Southern Illinois University, Carbondale, Illinois 62901-4401

P. V. Konarev

Department of Quantum Electronics, Moscow Engineering Physics Institute, Kashirskoe shosse 31, 115409 Moscow, Russia

M. Tischer

Hamburger Synchrotronstrahlungslabor, HASYLAB at DESY, Notkestraße 85, D-22603 Hamburg, Germany

A. V. Tsvyashchenko and L. N. Fomicheva

Vereshchagin Institute of High Pressure Physics, 142092 Troitsk, Moscow region, Russia

(Received 12 July 1999; revised manuscript received 22 September 1999)

We have performed Ni K -edge extended x-ray-absorption fine structure measurements on $\text{YNi}_2\text{B}_2\text{C}$ superconductor ($T_c \sim 15.2$ K) in the temperature range 5–220 K. The results show that local structure is distorted from a perfect $I4/mmm$ crystalline structure expected from diffraction measurements below $T_p \sim 60$ K. Two different Ni-Ni distances separated by ~ 0.09 Å may be extracted at 5 K. We argue that $\text{YNi}_2\text{B}_2\text{C}$ is inhomogeneous at the atomic length scale and discuss a possible reason for the observed distortions.

The quaternary intermetallic compounds of the recently discovered borocarbide family^{1,2} $\text{RNi}_2\text{B}_2\text{C}$ (R stands for rare-earth) have very interesting physical properties. Many compounds are superconducting, even those that contain magnetic rare-earth atoms such as Dy, Ho, and Er, which opens the road for a detailed study of the interplay between superconductivity and magnetism. The structure of these compounds primarily determined for $R=\text{Lu}$ is body-centered tetragonal³ (space group $I4/mmm$) and consists of R -C layers separated by Ni_2B_2 sheets. Further neutron-diffraction⁴ measurements show the $I4/mmm$ nuclear structure regardless of the temperature and rare-earth constituents. For $\text{YNi}_2\text{B}_2\text{C}$, of particular interest to the present study, the Ni atoms are tetrahedrally coordinated with four B atoms at 2.10 Å. Ni-Ni separation of 2.49 Å in the Ni layers is similar to the Ni metal interatomic distance (2.50 Å) so that Ni-Ni interactions will be strong. The layered structure and the $I4/mmm$ space group that is shared with several Cu-based superconductors as well as the covalent nature of bonding in the transition-metal borides and carbides raises the possibility that borocarbides might be two-dimensional (2D) high temperature superconductors that do not contain either copper or oxygen. However, self-consistent band structure calculations on $\text{LuNi}_2\text{B}_2\text{C}$ in the local-density approximation⁵ (LDA) show no obvious “few-bands” that summarize the electronic structure near the Fermi level. A remarkable peak at E_f was found to dominate by Ni $3d$ states with almost equal proportions of all five Ni $3d$ orbitals and also involves some Lu $5d$ and B, C s - p admixture, implying 3D rather than 2D character. Although the spectral weight measured by photoemission⁶ is in qualitative agreement with that calculated from LDA’s density of states, they are different in the vicinity of the Fermi level. As was pointed out by Fujimori *et al.*,⁶ it should be a mechanism for the spectral weight transfer away from E_f on an energy scale of 0.5–1 eV that may be reminiscent of pseudogap formation as has been pre-

dicted for strongly coupled electron-phonon systems⁷ and electrons interacting with spin fluctuations.⁸ A question of whether the $\text{RNi}_2\text{B}_2\text{C}$ family is in a weak- or strong-coupling regime is not yet settled. Specific heat studies indicate an intermediate-to-strong coupling with ($\lambda \sim 0.5$ – 1.0) (Ref. 9) and (~ 0.95 – 1.15),¹⁰ but tunneling measurements show the weak BCS-type regime.¹¹ In the BCS theory λ is the ratio of the interaction energy of the carriers with phonons that are responsible for the coupling of their kinetic energy to the kinetic energy. At $\lambda > 1$ the potential energy due to the lattice deformation exceeds the kinetic energy of the carriers. This is a condition for polaron formation that has been known for a long time as a solution for a single electron coupled with lattice vibrations.¹²

In this paper we report on Ni K -edge extended x-ray-absorption fine-structure (EXAFS) measurements of $\text{YNi}_2\text{B}_2\text{C}$ to study the temperature dependence of the local structure around the Ni sites. Being a direct and fast probe technique, EXAFS provides structural information on atomic length scales and, therefore, directly addresses possible polaron formation. $\text{YNi}_2\text{B}_2\text{C}$ is also particularly interesting because antiferromagnetic (AF) spin fluctuations have been observed by pulsed NMR (Ref. 13) which, like the EXAFS, is a local sensitive technique. One of the goals of our study is to establish correlations between the EXAFS and NMR results.

Polycrystalline samples of $\text{YNi}_2\text{B}_2\text{C}$ were synthesized and annealed as described elsewhere.¹ Phase purity was checked by powder x-ray diffraction. The sample is body-centered tetragonal with space group $I4/mmm$ and lattice parameters $a = 3.52(6)$ and $c = 10.54(2)$ Å at room temperature, consistent with previous diffraction measurements.¹⁴ The superconducting properties were investigated by dc susceptibility measurements using a superconducting quantum interference device magnetometer. Annealed samples show $T_c \sim 15.2$ K in a field of 30 G. X-ray-absorption measure-

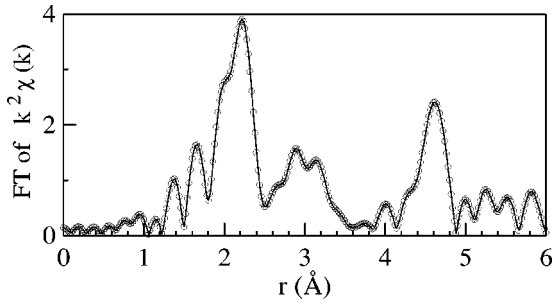


FIG. 1. Magnitude of the Fourier transform (FT) of the Ni K -edge EXAFS weighted by k^2 at 5 K. The FT range is $k = 1.55\text{--}17.94 \text{ \AA}^{-1}$, square window.

ments were performed in the transmission mode at HASY-LAB at DESY. Ni K -edge spectra were collected at beamline EXAFS-II using a Si(111) double crystal fixed-exit monochromator. The higher-order harmonics were suppressed by detuning the second crystal of the monochromator on its rocking curve to $\sim 40\%$ of the maximum transmitted intensity at the high-energy point taken at 1.4 keV above the ionization threshold. The energy resolution was estimated to be $\sim 2 \text{ eV}$ at an entrance slit of 0.7 mm. The samples were installed in an Oxford CF1204 flow cryostat with temperature monitored within $\pm 0.5 \text{ K}$. The standard procedures for experimental data reduction were used¹⁵ to obtain $k^2\chi(k)$ EXAFS spectra.

Figure 1 shows the magnitude of the Fourier transform (FT) of the $k^2\chi(k)$ EXAFS spectra taken at 5 K. In the present work we will focus only on the Ni-Ni and Ni-B distributions that appear as a first peak in the FT. There is no multiple scattering (MS) contribution to this area of r space because MS terms have longer photoelectron pathlengths that essentially simplify the data analysis and allow a clear physical interpretation: the peak is due to single scattering of photoelectron emitted by absorbing Ni atom by four nickel and four boron near-neighbor atoms and therefore it involves information on the pair distribution of Ni-Ni and Ni-B atoms. EXAFS from Ni-Ni and Ni-B pairs were isolated through a back FT (BFT) to k space (Fig. 2). The resulting data were then fitted with two site distributions ($R_{\text{Ni-Ni}} = 2.49 \text{ \AA}$ and $R_{\text{Ni-B}} = 2.10 \text{ \AA}$, respectively) as expected from diffraction measurements.¹⁴ The amplitudes and phase shifts were generated by FEFF6 code.¹⁶ A reasonably good fit was achieved: $R_{\text{Ni-B}} = 2.10 \pm 0.02 \text{ \AA}$ and the Debye-Waller (DW) factor, $\sigma_{\text{Ni-B}}^2 = 5.4 \pm 2.1 \times 10^{-3} \text{ \AA}^2$ over whole temperature range. Temperature dependence of the $\sigma_{\text{Ni-B}}^2$ extracted from our data agrees somewhat with that expected from the Raman-scattering measurements.¹⁷ $R_{\text{Ni-Ni}} = 2.49 \pm 0.01 \text{ \AA}$, however, the $\sigma_{\text{Ni-Ni}}^2$ deviates from its standard temperature dependence below 60 K as revealed from Fig. 3(a). This implies that the Ni-Ni pair distribution is distorted from the perfect $I4/mmm$ structure expected by diffraction measurements, being more complicated than the one-site distribution. It should be noted that the DW factor corresponding to the Ni-B bond is relatively large that, in turn, allows some Ni-B distribution. It is easy to show by means of direct EXAFS simulation that assuming a unique Ni site and two site B distributions it is not possible to achieve a good fit because correction is required predominantly in the higher k -space range, where the magnitude of boron contributions falls off

TABLE I. Local structure parameters obtained from the 1S and 2S fits. The number of neighbors, $N=4$ and $N_{\text{short}}=2.2$ with estimated errors of 15%. $S_0^2=0.8(1)$. The agreement factor, $R_a = 1/M \sum_i (\chi_i^{\text{exp}} - \chi_i^{\text{calc}})^2$, where M is a number of data points. For the fitting ranges of $3.5\text{--}17 \text{ \AA}^{-1}$ in k space and $1.2\text{--}2.4 \text{ \AA}$ in r space, the allowed number of the fitting parameters is 12 (Ref. 18). Numbers of degrees of freedom in the 1S and 2S fits are $\nu_1=9$ and $\nu_2=6$, respectively.

$T \text{ (K)}$		$R \text{ (\AA)}$	$\sigma^2 (10^3 \text{ \AA}^2)$	$R_a \times 10^3$
5	1s	$R = 2.481 \pm 0.005$	3.11 ± 0.16	7.0
5	2s	$\begin{cases} R_{\text{short}} = 2.450 \pm 0.009 \\ R_{\text{long}} = 2.536 \pm 0.011 \end{cases}$	$\begin{cases} 0.61 \pm 0.14 \\ 1.08 \pm 0.21 \end{cases}$	4.2
20	1s	$R = 2.482 \pm 0.006$	1.62 ± 0.17	8.9
20	2s	$\begin{cases} R_{\text{short}} = 2.465 \pm 0.010 \\ R_{\text{long}} = 2.506 \pm 0.010 \end{cases}$	$\begin{cases} 0.72 \pm 0.16 \\ 1.08 \pm 0.24 \end{cases}$	8.1
40	1s	$R = 2.481 \pm 0.005$	2.30 ± 0.12	5.9
40	2s	$\begin{cases} R_{\text{short}} = 2.461 \pm 0.010 \\ R_{\text{long}} = 2.519 \pm 0.010 \end{cases}$	$\begin{cases} 0.74 \pm 0.12 \\ 1.40 \pm 0.20 \end{cases}$	4.8
220	1s	$R = 2.489 \pm 0.008$	5.12 ± 0.30	7.8

much faster than the nickel one. This implies that disorder in the Ni-B pair is presumably at a Ni site, consistent with the results of NMR (Ref. 13) where one crystallographic B site was observed. Therefore, one can focus on the Ni-Ni distribution.

We performed constrain fits using three and six parameters for one-site (1S) and two-site (2S) Ni-Ni distributions and keeping three parameters of Ni-B distribution fixed as they extracted from the primary fit. For the 2S model the parameters were R_{short} , R_{long} , two DW factors, N_{short} ($N_{\text{long}} = 4 - N_{\text{short}}$), and one energy shift, ΔE for the split Ni-Ni distances. The results of the refinement at several temperatures are summarized in Table I. Since the $R_a^{2S}/\nu_2 < R_a^{1S}/\nu_1$ at two lowest temperatures of 5 and 9 K, the 2S models do improve the goodness of the fits and, therefore, two different Ni-Ni distances can be extracted. The 2S model, indicated by a dashed line in Fig. 2 shows an excellent agreement with the BFT data. An average Ni-Ni distance agrees reasonably well with that from the diffraction data. This implies that the long range order in the Ni-layers may be understood as a superimposed average of two different local Ni-Ni bonds. It is worth mentioning that local struc-

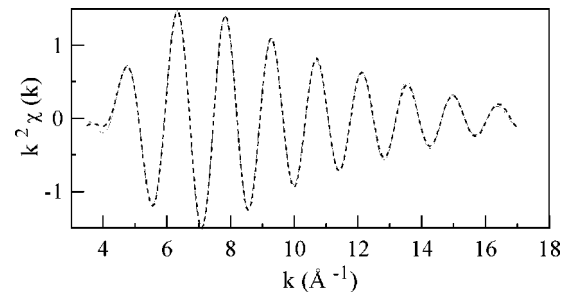


FIG. 2. Comparison of the Fourier filtered contribution from Ni-Ni and Ni-B bonds (solid line) with the fitting curve corresponding to the constrain 2S model assuming two-site Ni-Ni distribution, $T = 5 \text{ K}$.

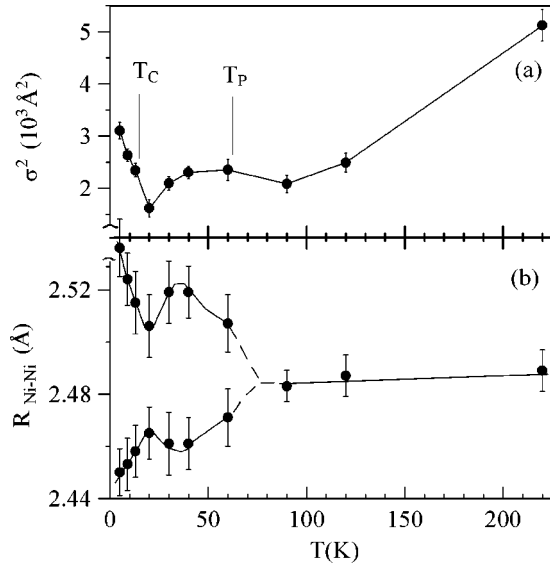


FIG. 3. Temperature dependencies: (a) of the DW factor corresponding to the one-site Ni-Ni distribution; (b) the Ni-Ni distance split extracted from the 2S model. All lines are guides to the eye.

ture distortions *coexist* with superconductivity. Instead, at 13 K and higher temperatures the best fits are given by the one-site Ni-Ni distributions, though the DW factors increase with temperature decreases below 60 K. In this case the 2S fits still provide an estimation for the upper limits of the Ni-Ni bond distortions. As revealed from Fig. 3(b) two different distances may be extracted up to $T_p \sim 60 \text{ K}$, that correlates with an onset of the anomaly DW factor behavior in the 1S model. We would like to mention that the large value of the DW factor of the one-site distribution and its unexpectedly fast growth with temperature, $\sigma^2(220 \text{ K}) - \sigma^2(60 \text{ K}) \sim 2.3 \times 10^{-3} \text{ \AA}^2$ against $1.1 \times 10^{-4} \text{ \AA}^2$ estimated from the Einstein model¹⁹ with $\theta_E = 282 \text{ cm}^{-1}$ (Ref. 17) would argue in favor of the multiple site distribution even at $T > T_p$. Further work has to be done to elaborate on this point.

Intriguing, that regardless of the models the Ni-Ni distribution becomes almost homogeneous at $T_{cp} \sim 20 \text{ K}$, just above T_c . For the 2S model this appears as a minimum in the split that is relatively small but beyond the uncertainty of the fit. Unfortunately, the density of experimental points is not enough to draw up unambiguously how far T_{cp} is from T_c . Diffraction measurements did not observe any structural phase transitions down to 1.5 K.⁴ Therefore, these changes are on the atomic length scale. We suggest the minimum to be attributed to a locally correlated motion of Ni atoms in the vicinity of T_c . This situation may be qualitatively explained using a pair distribution function (PDF) which is related to structural parameters derived from the EXAFS fit as: $g(r) = \sum_i N_i / (\sqrt{2\pi}\sigma_i) \exp[-(r - R_i)^2 / 2\sigma_i^2]$. Ni-Ni PDFs generated from the 2S data set at several temperatures of interest are shown in Fig. 4, indicating essentially the two-site distribution in the superconducting phase ($T = 5 \text{ K}$) that still persists below $T_p \sim 60 \text{ K}$ though it looks like an asymmetric one-site distribution ($T = 40 \text{ K}$), and finally, converges to Gaussian distribution ($T = 220 \text{ K}$). The PDF width reflects the relative displacement of the atomic pair. If the near-neighbor atoms tend to move in phase with each other the PDF would appear as a sharp peak. That is exactly what is

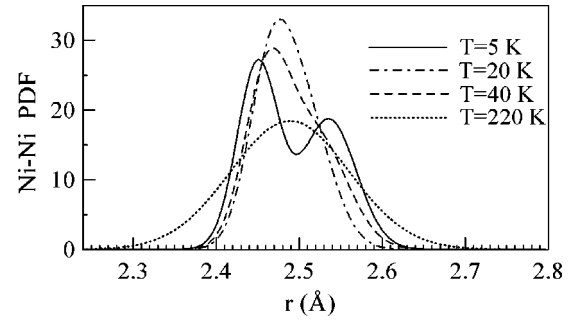


FIG. 4. Ni-Ni pair distribution functions vs temperature generated in the assumption of the Ni-Ni split indicated in Fig. 3(b).

seen in the PDF at $\sim 20 \text{ K}$ as indicated by dot-dashed line, when two peaks are about to merge into a single narrow peak and, therefore, to almost restore homogeneity of the sample on the atomic length scales.

Additional evidence for correlated Ni-Ni motion comes from the comparative analysis of experimental and calculated Ni K -edge x-ray absorption near edge structure (XANES), similar to that reported for NdCeCuO superconductor.²⁰ Ni K -edge data were collected with an improved energy resolution of $\sim 1 \text{ eV}$ at 5 K in order to minimize effects of thermal motion. We performed extensive multiple scattering calculations and found out that the shape of the calculated XANES corresponding to completely uncorrelated displacements seems to be very smooth compared to that of the experimental spectrum, indicating that the Ni atomic displacements are partially correlated.

Both present EXAFS studies and the NMR measurements point to a local inhomogeneity of $\text{YNi}_2\text{B}_2\text{C}$ at low temperatures. Two ^{11}B resonances are clearly observed below T_c . One of them was reported to come from a “normal-metal” region, while the other one comes from a superconducting region. This phase separation was attributed to the local non-stoichiometry at B and C sites at a microscopic level.¹³ Interpretation presented here is different. The distortions observed from EXAFS involve too many atoms to be entirely associated with imperfections. Indeed, the major variation in local structure is related to relative displacement within the Ni layers where Ni atoms do not alternate with B(C) ones. Two groups of Ni-Ni distances separated by $\sim 0.09 \text{ \AA}$ occur over the whole lattice. The next, and most important argument, is that the Ni-Ni displacements are correlated in the real space, as we have shown above. The imperfections must be randomly space distributed, otherwise the additional diffraction peaks from their ordering would be observed experimentally, that has never been reported to our knowledge. It is clear that uncorrelated imperfections *alone* could not be a driving force for the correlated displacements. We suggest that the local inhomogeneity at low temperatures is an endemic property of $\text{YNi}_2\text{B}_2\text{C}$.

The experimental results of NMR measurements provide valuable insight into the nature of the distortion in $\text{YNi}_2\text{B}_2\text{C}$. The temperature dependence of the $(T_1 T)^{-1}$ relaxation rate in the normal state can be described in terms of itinerant AF spin fluctuations.¹³ It is worth mentioning that there are no magnetic ions in $\text{YNi}_2\text{B}_2\text{C}$ except for the Ni ones. The only explanation for the observed AF spin fluctuation is to assume that the Ni atoms carry small moments. This Ni moment is

not easily captured by conventional neutron diffraction. Powder-diffraction data on $\text{YNi}_2\text{B}_2\text{C}$ (Ref. 21) placed an upper limit of $0.13\mu_B$ for the possible Ni magnetic moment associated with any antiferromagnetic ordering. However, a search for the local magnetic moment was performed assuming perfect $I4/mmm$ structure. In order to capture a magnetic moment on the *displaced* Ni ions one needs to analyze magnetic peaks up to a momentum transfer $Q \sim 30\text{--}40 \text{ \AA}^{-1}$ while in Ref. 21 the data were collected for $Q < 1.6 \text{ \AA}^{-1}$. Thus, neutron-diffraction observations do not contradict the presence of a small magnetic moment at the displaced Ni sites.

Remarkably, there is a clear correlation between the temperature dependence of nuclear relaxation rate deduced from NMR experiments above T_c and the temperature dependence of Ni-Ni splitting extracted from EXAFS. The relaxation rate is proportional to the magnitude of the AF spin fluctuations, which, in turn, is proportional to an effective local magnetic moment at the Ni site. The larger the effective local magnetic moment is the stronger the lattice distortions are. We speculate that this correlation reflects a tight relationship between the lattice and magnetic degrees of freedom and may be explained in terms of spin-polaron formation.²² Perhaps two magnetic moments belonging to near-neighbor Ni atoms align ferromagnetically and form a core that is dressed with a group of antiparallel oriented moments. The approach of Ni atoms within the core area lowers the electronic energy due

to enhancement of the exchange interaction but raises the lattice deformation energy. The number of moments involved seems to be small, because the polaronic mass increases exponentially with the number of its constituents, suppressing its mobility. In order to reconcile the good metallic conductivity with spin-polaron formation, we propose that the spin polarons spread over a few unit cells and are dynamic in this region. The dynamic nature of the spin polarons is also tentative because the exchange energy between coupled spins is of the same order of magnitude as the phonon energy. Therefore, the lattice dynamics may significantly interplay with the magnetic dynamics. This question as well as the details of spin-polaron formation require further studies.

In conclusion, we have observed the local structure of $\text{YNi}_2\text{B}_2\text{C}$ superconductor to be distorted within the Ni layers below $T_p \sim 60 \text{ K}$. It can be modeled assuming a two-site Ni-Ni pair distribution at 5 and 9 K and anomalously broadened one-site distribution between 13 and 60 K. The temperature dependence of the PDF indicates a correlated motion of Ni-Ni pairs in the vicinity of T_c . EXAFS observations combined with the NMR results¹³ provide supporting evidences for spin-polaron formation at low temperatures.

The authors are grateful to A. A. Ivanov for help in the measurements. This work was supported by the Consortium for Advanced Radiation Sources (University of Chicago).

¹R. J. Cava *et al.*, Nature (London) **367**, 252 (1994).

²R. Nagarajan *et al.*, Phys. Rev. Lett. **72**, 274 (1994).

³T. Siegrist *et al.*, Nature (London) **367**, 254 (1994).

⁴J. W. Lynn *et al.*, Phys. Rev. B **55**, 6584 (1997).

⁵L. F. Mattheiss, Phys. Rev. B **49**, 13 279 (1994).

⁶A. Fujimori *et al.*, Phys. Rev. B **50**, 9660 (1994).

⁷K. M. Ho *et al.*, Phys. Rev. Lett. **41**, 815 (1978).

⁸A. Kampf and J. R. Schieffer, Phys. Rev. B **41**, 6399 (1990).

⁹S. A. Carter *et al.*, Phys. Rev. B **50**, 4216 (1994).

¹⁰H. Michor *et al.*, Phys. Rev. B **52**, 16 165 (1995).

¹¹M. Xu *et al.*, Physica C **235-240**, 2533 (1995).

¹²See, for example, A. S. Alexandrov, Phys. Rev. B **46**, 2838 (1992), and references therein.

¹³T. Kohara *et al.*, Phys. Rev. B **51**, 3985 (1995).

¹⁴C. Godart *et al.*, Phys. Rev. B **51**, 489 (1995).

¹⁵T. M. Hayes and J. B. Boyce, in *Solid State Physics*, edited by H. Ehrenreich, F. Seitz, and D. Turnbull (Academic, New York, 1982), Vol. 37, p. 173.

¹⁶S. I. Zabinsky *et al.*, Phys. Rev. B **52**, 2995 (1995).

¹⁷V. G. Hadjiev *et al.*, Phys. Rev. B **50**, 16 726 (1994).

¹⁸E. A. Stern, Phys. Rev. B **48**, 9825 (1993).

¹⁹E. Seivillano *et al.*, Phys. Rev. B **20**, 4908 (1979).

²⁰A. Yu. Ignatov *et al.*, J. Synchrotron Radiat. **6**, 767 (1999).

²¹S. K. Sinha *et al.*, Phys. Rev. B **51**, 681 (1995).

²²N. F. Mott, J. Phys.: Condens. Matter **5**, 3487 (1993).